J Mater Sci (2008) 43:3825–3831
DOI 10.1007/s10853-007-2291-5

Ab initio investigation of twin boundary motion in the magnetic shape memory Heusler alloy Ni_2MnGa

Markus E. Gruner · Peter Entel · Ingo Opahle · Manuel Richter

Received: 7 July 2007 / Accepted: 1 November 2007 / Published online: 13 March 2008

Abstract Magnetic shape memory (MSM) alloys, which transform martensitically below the Curie temperature in the ferromagnetic (FM) state, represent a new class of actuators. In Ni_2MnGa, unusually large magnetic field-induced strains of about 10% have been observed. This effect is related to a high mobility of martensitic twin boundaries in connection with a large magneto-crystalline anisotropy. MSM materials exist in a variety of different martensitic structures depending on temperature and compositions. We investigate the energetics of $L1_0$ phase twin boundary motion quasi-statically with ab initio methods and relate the results to calculations of the magneto-crystalline anisotropy energy. Our results indicate that for the $L1_0$ structure the energy needed for a coherent shift of a twin boundary may be too large to be overcome solely by magnetic field-induced strains.

Introduction

In the martensitic phase of the magnetic shape memory (MSM) Heusler alloy Ni_2MnGa, strains of up to 10% can be induced by external magnetic fields, making the material a technologically relevant candidate for magneto-mechanical actuators [1–3] (for a recent review of theoretical work on Ni_2MnGa, see [4]). The MSM effect in near stoichiometric Ni_2MnGa is attributed to a high mobility of the twin boundaries in connection with a large magneto-crystalline anisotropy in the martensitic phase. The effective stress induced by the external magnetic field allows for the reorientation of martensitic twins thereby changing the shape of the crystal. Therefore, the large magneto-crystalline anisotropy in the martensitic phases together with the low activation energy for twin boundary motion is considered a key ingredient for the reversible growth of one martensitic variant at the expense of another in MSM alloys leading to the large reported strains. This MSM mechanism is usually referred to as *magnetic field-induced reorientation* (MIR). There is another mechanism called *magnetic field-induced martensite* (MIM), which can occur when martensitic and magnetic phase boundaries are coupled. Such transitions do not necessarily require large uniaxial magneto-crystalline anisotropies and a high mobility of twin boundaries, but rather a martensitic transition temperature in the desired operation range and a large change in magnetization between both phases. A sufficiently strong magnetic field can then shift the martensitic transition temperatures and thus reversibly induce a martensitic transition. This effect was observed in polycrystalline Ni–Mn–In with a magnetic field-induced strain comparable to other polycrystalline MSM alloys [5, 6].

While near stoichiometric Ni_2MnGa shows cubic $L2_1$ symmetry in the austenitic phase, the martensitic phase is characterized by modulated pseudo-tetragonal and orthorhombic structures with $c/a \approx 0.94$ and a body-centered tetragonal (bct) $L1_0$ structure with $c/a > 1$ depending on temperature and composition [7]. So far, the origin of the high mobility of the twin boundaries in the modulated phases is unresolved and empirical potentials incorporating magnetism permitting the simulation of twin boundary

M. E. Gruner (✉) · P. Entel
Physics Department, University of Duisburg-Essen,
47048 Duisburg, Germany
e-mail: Markus.Gruner@uni-duisburg-essen.de

I. Opahle · M. Richter
IFW Dresden, P.O. Box 270116, 01171 Dresden, Germany

motion on the relevant length and time scales do not exist. We therefore attempt to close this gap by large scale ab initio calculations in the framework of density functional theory allowing the investigation of simplified models of martensitic twin boundaries for the different martensitic structures of Ni_2MnGa with the help of contemporary supercomputers. As a first step, we examine the shear-induced mobility of twin boundaries in the bct $L1_0$ phase and compare our results to calculations of the magneto-crystalline anisotropy energy.

Computational details

The simulations have been carried out from first principles within the framework of density functional theory (DFT) using the Vienna Ab Initio Simulation Package (VASP). This employs a plane wave basis set and the projector augmented wave (PAW) pseudopotentials [8, 9] providing an excellent compromise between the speed of calculations and accuracy. We used pseudopotentials with $3d^9 4s^1$ as valence for Ni, $3d^6 4s^1$ for Mn, and $4s^2 4p^1$ for Ga and a spin polarized representation of the electronic charge densities allowing for collinear description of magnetic moments. The exchange correlation potential was treated within the Generalized Gradient Approximation (GGA) using the formulation of Perdew, Burke, and Ernzerhoff [10]. Due to the large simulation cell, *k*-point integration was restricted to the Γ-point only. The plane wave cutoff was set to 337 eV. The geometric relaxations performed using the conjugate gradient method were carried out until difference between total energies of two consecutive steps fell below 0.1 meV.

For the calculation of the magneto-crystalline anisotropy energies (MAE) a very high accuracy is mandatory. Therefore, we employed the full-potential local-orbital minimum-basis package FPLO (version 5.00-19) [11–13] for this task providing a 4-component code for calculating relativistic effects [14]. The basis set used in the calculations consisted of 3d and 4sp electrons as valence for Ni, Mn, and Ga, while the 3sp electrons were treated as semi-core states. The exchange correlation functional was used in the local spin density approximation (LSDA) with the parameterization of Perdew and Wang [15]. The spin–orbit calculations were performed selfconsistently for each quantization direction. For the *k*-space integration, 13,824 points in the full Brillouin zone proved to be sufficient, assuring that the energies are converged within 5 μeV/f.u. and the orbital moments within 10^{-4} μ_B. Since there is no marked dependence of the equilibrium volume on the *c/a* ratio, the GGA and the LSDA calculations were carried out at the respective equilibrium volume of the $L2_1$ phase.

Magneto-crystalline anisotropy in Ni_2MnGa

The MAE of Ni_2MnGa has been previously reported by Enkovaara et al. [16] for *c/a* ratios ranging from 0.92 to 1.05. The authors found a nearly linear dependence of the MAE with respect to the *c/a* ratio, which passes zero at $c/a = 1$, due to symmetry reasons. This raises expectations that considerably larger MAEs may be encountered for the $L1_0$ phase with $c/a \approx 1.25$, than for the modulated phases with $c/a \approx 0.94$. Therefore, we carried out calculations up to $c/a = 1.25$, which is close to the absolute energy minimum of the $L1_0$ phase, manifesting the theoretical energetic ground state of Ni_2MnGa. Our results are summarized in Fig. 1. The lower panel refers to the variation of the total energy relative to the cubic $L2_1$ phase with the *c/a* ratio without spin–orbit interactions, exhibiting a deep minimum close to $c/a = 1.25$. The upper panel shows the energies for various spin quantization directions relative to the energy with moments aligned along the *c*-axis. Our values for $0.95 \leq c/a \leq 1.05$ agree well with the results published in [16]. For $c/a < 1$ the [001] axis is the easy direction while it becomes the hard axis for $c/a > 1$. In the latter case, the total energies calculated for the [010] and [110] quantization axes are lowest and degenerate, resulting in an easy plane magneto-crystalline anisotropy for $c/a > 1$. The [111] and [011] directions are intermediate,

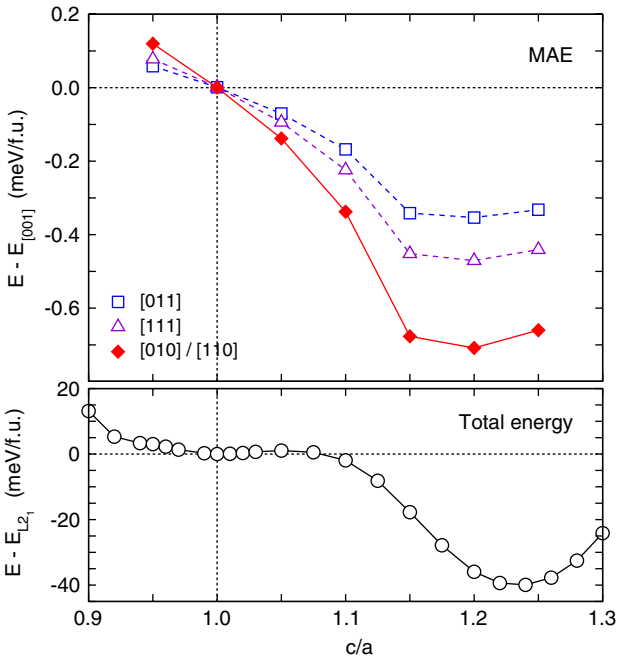

Fig. 1 Magneto-crystalline anisotropy energies per formula unit of Ni_2MnGa for different quantization directions and *c/a* ratios as obtained by the FPLO code. The energies are specified relative to the [001] quantization axis, which is the easy axis for $c/a < 1$. The total energy as a function of the *c/a* ratio calculated without spin–orbit interactions is shown in the lower panel

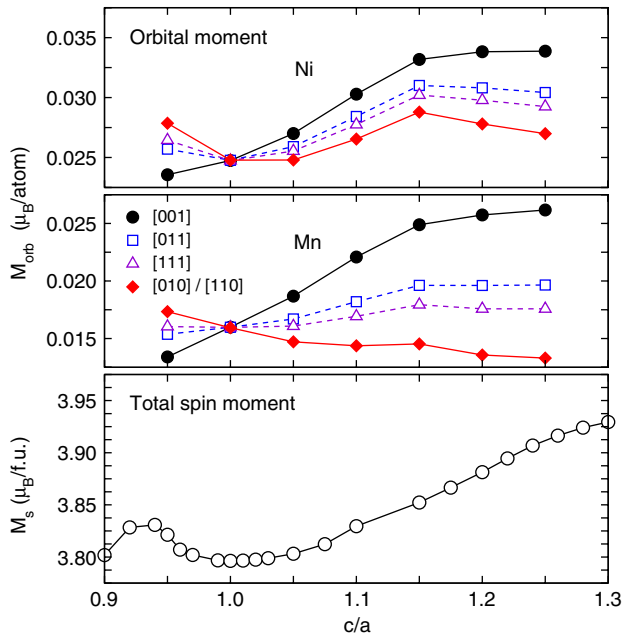

Fig. 2 Element specific orbital moments of Ni and Mn for different quantization directions and *c*/*a* ratios obtained by the FPLO code. The lower panel displays for comparison the total spin moment of the unit cell. It should be noted, that due to the smaller equilibrium volume caused by the overbinding of the LDA, the moments are about 6% smaller than those obtained within the GGA

neither referring to easy nor hard axes and included for the sake of completeness. The maximum MAE of 0.7 meV/f.u. is reached for $c/a \approx 1.20$.

The corresponding orbital and spin moments can be found in Fig. 2. For the [001] quantization axis, both the Ni and the Mn orbital moments have a marked dependence on the *c*/*a* ratio. The orbital moment of Mn at $c/a = 1.25$ is nearly doubled with respect to the value at $c/a = 1$. For the [010] and [110] axes, this dependence is much less pronounced. For the Ga sites, the calculated orbital moments are insignificant. The orbital moment anisotropy (OMA) is given by the difference in the orbital moments between the easy axis and the hard axis alignment of the magnetization. For $c/a = 0.95$, the contributions of the individual Mn and Ni atoms are of the same magnitude, suggesting, following the argument given in [16], that the MAE is dominated by the Ni species (which appears twice in the unit cell) in this case. For $c/a = 1.25$ the contribution of the Mn atoms to the OMA increases to almost twice the contribution of the Ni species, indicating a comparable influence of Mn in this *c*/*a* range.

Modeling twin boundary motion

As a material undergoes a martensitic transformation from a high symmetry parent phase at higher temperatures to a low-symmetry low-temperature phase, so-called twinning will occur. In MSM Heusler alloys, such as Ni_2MnGa, the parent phase is characterized by the cubic $L2_1$ symmetry, while for the martensitic phase it is either the tetragonal $L1_0$ symmetry with $c/a > 1$, or, respectively, the modulated, pseudo-tetragonal 10 M (5 M) or monoclinic 14 M (7 M) structures with $c/a < 1$. Within this study, as a first step, we concentrate on the simulation of $L1_0$ twin boundary with $c/a = 1.25$, which is close to the ground state for Ni_2MnGa as obtained by ab initio calculations [17, 18] and thus potential difficulties connected with the meta-stability of the modulated martensitic phases do not arise.

Mathematically, the transition can be described by a simple homogeneous transformation, characterized by a matrix $\underline{\underline{F}}$ and a vector $\underline{c}$ (or $\underline{\underline{G}}$ and $\underline{d}$, respectively) and, possibly, by an additional shuffle (for a detailed introduction to the continuum theory of martensitic transformations in shape-memory materials, see [19–21]). The martensitic twins are, in general, represented by different homogeneous transformations, typically connected by symmetry operations, e.g., a rotation $\underline{\underline{Q}}$, which is part of the point group of the parent phase but not of martensite. With the condition of kinematic compatibility, assuring that a line crossing the twin boundary remains unbroken (but will be kinked), it follows:

$$\underline{\underline{QF}} - \underline{\underline{G}} = \underline{a} \otimes \underline{\hat{n}}. \tag{1}$$

The vector $\underline{a}$ and the normal vector of the twin boundary plane $\underline{\hat{n}}$ are given by the following equations

$$\underline{a} = |\underline{n}| \left(\sqrt{\frac{\lambda_3(1-\lambda_1)}{\lambda_3-\lambda_1}}\underline{\hat{e}_1} \pm \sqrt{\frac{\lambda_1(1-\lambda_3)}{\lambda_3-\lambda_1}}\underline{\hat{e}_3} \right), \tag{2}$$

$$\underline{\hat{n}} = \frac{1}{|\underline{n}|} \frac{\sqrt{\lambda_3}-\sqrt{\lambda_1}}{\sqrt{\lambda_3-\lambda_1}} \left(-\sqrt{1-\lambda_1}\underline{\underline{G}}^{\mathrm{T}}\underline{\hat{e}_1} \pm \sqrt{\lambda_3-1}\underline{\underline{G}}^{\mathrm{T}}\underline{\hat{e}_3} \right), \tag{3}$$

if an ordered set of eigenvalues $\lambda_1 \le \lambda_2 = 1 \le \lambda_3$ of $\underline{\underline{C}} = \underline{\underline{G}}^{-\mathrm{T}}\underline{\underline{F}}^{\mathrm{T}}\underline{\underline{F}}\underline{\underline{G}}^{-1}$ exists [22]; $\underline{\hat{e}_1}$ and $\underline{\hat{e}_3}$ refer to the corresponding eigenvectors. This relation can be used to construct a model of a martensitic twin boundary suitable for atomistic simulations as depicted in Fig. 3. Compatibility with the periodic boundary conditions can be achieved by rotating the system so that the twinning plane given by $\underline{\hat{n}}$ is parallel to one of the boundary planes of the simulation cell. The periodic boundary conditions also imply that there are at least two twin boundaries in the simulation cell. For the transformation to the $L1_0$ structure, the transformation matrix can be chosen in analogy to the Bain-path [23] as a (volume conserving) diagonal matrix with one of the diagonal elements different from the other two.

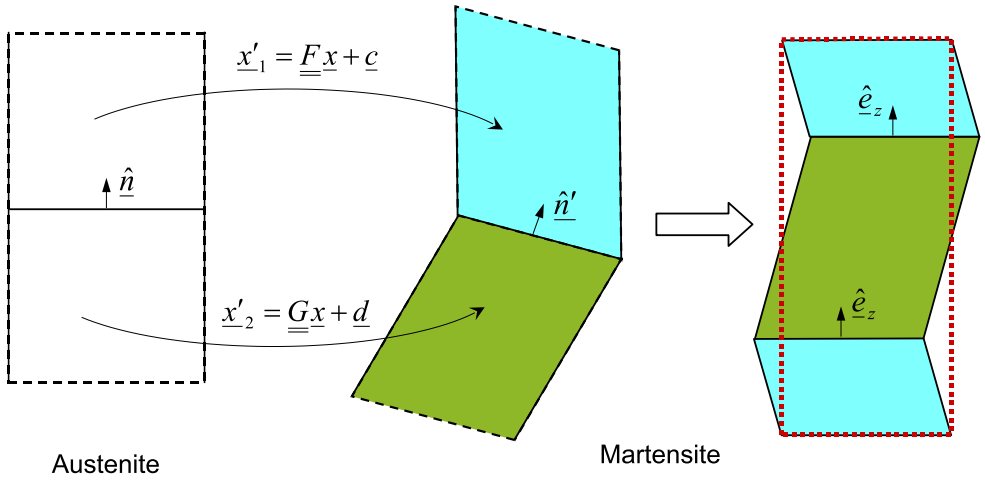

Fig. 3 Construction of an atomistic twin boundary model compatible with periodic boundary conditions. The martensite variants (denoted by primed coordinate vectors $\underline{x}'_1$ and $\underline{x}'_2$) are created from the austenitic phase by homogeneous transformations described by the matrices $\underline{\underline{F}}$ and $\underline{\underline{G}}$ and the vectors $\underline{c}$ and $\underline{d}$, respectively. To achieve the compatibility with the periodically repeated simulation super-cell, which is shaped as a parallelepiped, a rotation of the twinning plane given by the normal vector $\hat{\underline{n}}'$ is necessary, so that it is parallel to one pair of the boundary surfaces of the super-cell (here, with the normal $\hat{\underline{e}}_z$). By this step, a second twin boundary is introduced

The direct ab initio molecular dynamics simulation of twin boundary motion induced by a directional change of magnetic field must be considered as too expensive at the current stage since this would require the inclusion of spin–orbit interactions which slows down the self-consistency iteration process considerably. However, coherent twin boundary motion can also be induced mechanically by applying shear on the simulation cell. The induced strain will be partially resolved in a subsequent relaxation step, as sketched in Fig. 4, possibly leading to the introduction of defects or a shift of the twining plane. Then, in a sequence of consecutive shear and relaxation steps, a quasi-static picture of twin boundary motion can be achieved. This allows for the estimation of total energies as a function of the shear and the monitoring of changes in the magnetic properties given by the splitting of the majority and minority spin contributions of the electronic charge density, neglecting spin–orbit contributions in a first step.

The result of such a procedure is shown in Fig. 5. Here, we used a supercell containing 256 atoms and two martensitic variants with a width of two unit cells each, which is the smallest possible system size for studying twin boundary motion. The energies are related to the movement of two twin boundaries with a base area of 1.078 nm × 1.726 nm; the height of the simulation cell is 1.684 nm. The variants possess $L1_0$ structure with $c/a = 1.25$, which corresponds to the absolute minimum of the calculated energy landscape for Ni_2MnGa. The individual spin moments of atoms near the interface show only small deviations from their bulk value, comparable to the uncertainty due to finite size effects. Applying a shear to the simulation cell first increases the energy of the system without considerable effect on the location of the twin boundary. At a critical value, a coherent sliding of the lattice planes along the direction of the shear is observed before it snaps into another configuration where the height of one twin is enlarged by one unit cell at the

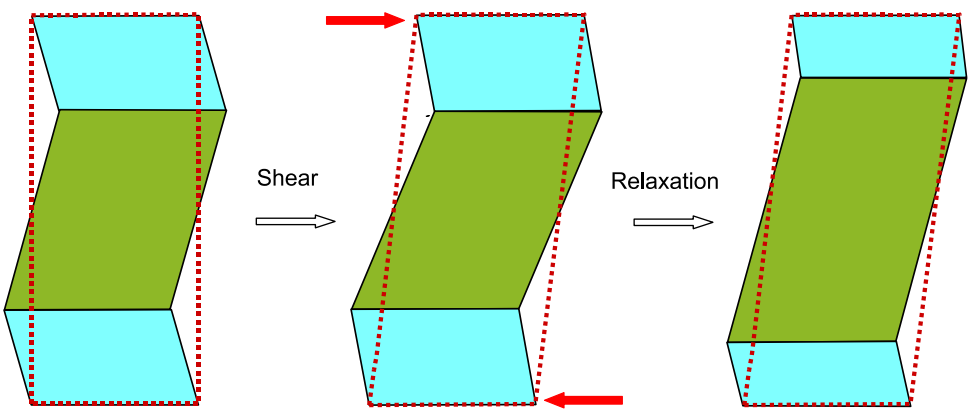

Fig. 4 Schematic sketch of the simulation of twin boundary movement as performed in our calculations consisting of multiple shearing of the super-cell with subsequent relaxation of the atomic positions

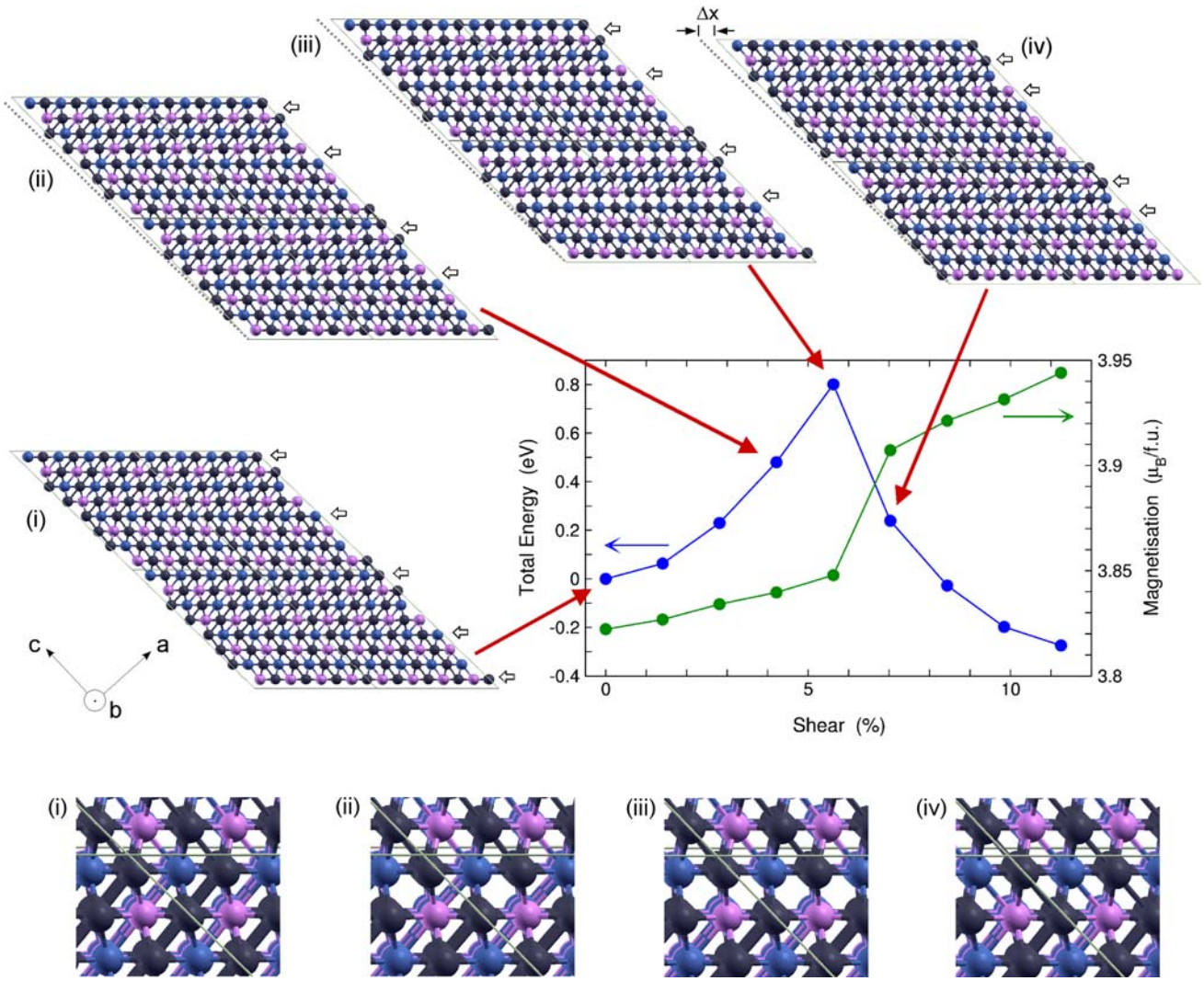

Fig. 5 Motion of a twin boundary and the corresponding energies and magnetizations obtained by eight subsequent shear and relaxation steps. Total energy and magnetic moment are given as a function of the shear of the simulation cell for each completed quasistatic relaxation step. The configurations (i)–(iv) which are arranged around the graph represent the results of the geometric optimization processes at the respective shear of the simulation box, which is applied in horizontal direction. To give a better impression of the processes at both twin boundaries, the simulation cell is doubled horizontally and vertically; the twin boundaries are marked by open arrows. The broken lines depict the initial inclination of the *c*-axis corresponding to the leftmost simulation cell. The corresponding shear is given by the shift Δx divided by the height of the cell. The atoms in the third dimension are hidden behind the topmost layer. Black spheres denote the Ni atoms, while blue and bright purple denote Mn and Ga, respectively. Between pairs of atoms, bonds are drawn if their distance is shorter than a threshold value of 2.835 Å visualizing the shortening of the crystal axis *a* in the respective direction. The bottom row shows enlarged views of the interfaces taken from the central part of the respective configurations (i)–(iv)

expense of the other. The process of sliding marks a transition state with maximum energy. Here, a regular, nearly square pattern of Ni, Mn, and Ga atoms is visible in the projection along the twin boundary, with the width of one half of the unit cell. The respective *c*- and *a*-axes remain larger than the *b*-axis, so that the three-dimensional pattern is not cubic but (approximately) tetragonal.

It can also be seen from Fig. 5 that the energy of the final state is lower than that of the initial state and possesses a considerably larger magnetic moment. This can be regarded as an artifact of the finite system size which obviously does not allow to effectively prevent interactions between the twin boundaries, so that the energy of the transition state can only be used as a very rough measure for the activation energy of a coherent twin boundary sliding process. Nevertheless, an estimation of the impact of a magnetic field on the stability of the twin boundaries can be already attempted at this stage. The energetically most favorable state for the configurations depicted in Fig. 5 should be a spin quantization axis pointing out of the

viewing plane, which suits both the martensitic variants. However, with a sufficiently strong magnetic field, the magnetization can be forced into the plane, parallel to an easy axis of one of the variants. For the other variant, the moments are aligned in direction of (but not entirely parallel to) its hard axis. So the accumulated MAE of the atoms along the twin boundary can be regarded as a measure of driving force for a field-induced reorientation process as sketched above. In fact, the activation energy turns out to be more than one order of magnitude larger than the MAE per atom, as obtained from Fig. 1, multiplied with the system size. Furthermore, the structural pattern occuring at the twin boundary in the transition state possess a shortened *b*-axis which may result in a preference for an out of plane alignment of the magnetization. In conclusion, our results indicate that the coherent magnetic field-induced reorientation is not a realistic process for stoichiometric $L1_0$ Ni_2MnGa with a large *c*/*a* value. However, the interface studied here is by construction planar and defect-free. It has been shown that interface defects with dislocation and step character play a decisive role in so-called military, plane-by-plane transformations (see [24] for a topical review). Disconnections can move at lower stresses than complete lattice planes and should therefore be paid attention to in a realistic modeling of twin boundary motion processes. This requires simulations of much larger systems which is currently not feasible using ab initio methods. In ordered stoichiometrical Ni_2MnGa, the detailed mechanism of twin boundary motion is not resolved yet. The simplified approach presented here provides a basis for a systematic comparison between the energy scales of twin boundary motion in different phases and compositions.

Conclusion and outlook

Within this work, we present an example of how to get microscopic insight into a stress-induced martensitic reorientation process in Ni_2MnGa by means of ab initio molecular statics calculations. Due to the importance of the electronic structure, simpler empirical model approaches are not applicable, so that this can only be done with density functional theory methods which require large amount of computational power so that the simulations are restricted to comparatively small system sizes and defect-free interfaces. The relativistic calculations including spin–orbit terms reveal that the MAE in the bct $L1_0$ phase at $c/a \geq 1.2$ is by far larger than in the pseudo-tetragonal phases with $c/a < 1$. On the other hand, the former easy axis becomes the hard axis of magnetization in this case, resulting in a plane of easy directions. Relating these results to the quasistatic simulations of shear-induced twin boundary motion in the $L1_0$ phase, we see, however, that the energy scales encountered in the coherent reorientation processes of twins and magnetization are not of the same order of magnitude. This is in accordance with recent energetic considerations by Kakeshita et al. [25–27] based on the data obtained from experimental studies of $Ni_{2.14}Mn_{0.92}Ga_{0.94}$ in the $L1_0$ phase with $c/a \approx 1.20$. It was shown for this composition that the stress necessary for twinning plane movement is one order of magnitude larger than the magnetic shear stress acting across a twinning plane, while this relationship is reversed for the stoichiometric composition in the 10 M phase, where in fact MSM behavior is observed.

Therefore, the more intriguing problem is certainly the energetics of twin boundary motion in the modulated martensitic phases with $c/a < 1$, which is expected to happen on a much smaller energy scale. In this case, however, technical problems concerning the stability of these phases at zero temperature can be expected, so that simulations at finite temperatures may be required, increasing the numerical and methodological effort. Another interesting aspect is the investigation of field-induced martensitic transformations occuring away from stoichiometry in Ni–Mn–Ga, Ni–Mn–In and Ni–Mn–Sn alloys. In off-stoichiometric $Ni_{2+x}Mn_{1-x}Ga$, where the phase transition between the $L2_1$- and $L1_0$-phase and the magnetic transition line coincide, fixed spin moment calculations will be useful to understand MSM effects by magnetic field-induced martensite.

Acknowledgements We would like to thank U. K. Rößler for helpful discussions and a careful proofreading of the manuscript. Large parts of the calculations were performed on the IBM Blue Gene/L supercomputer of the John von Neumann Institute for Computing at Forschungszentrum Jülich, Germany. We thank the local staff for their support and Dr Pascal Vezolle of IBM for his efforts in optimizing the VASP binary for the Blue Gene/L architecture. The atomistic visualizations in Fig. 5 were prepared using XCrySDen [28]. Financial support was granted by the Deutsche Forschungsgemeinschaft through the Priority Programme SPP1239, *Change of microstructure and shape of solid materials by external magnetic fields*.

References

1. Ullakko K, Huang JK, Kantner C, O'Handley RC, Kokorin VV (1996) Appl Phys Lett 69:1966
2. Sozinov A, Likhachev AA, Lanska N, Ullakko K (2002) Appl Phys Lett 80:1746
3. Söderberg O, Ge Y, Sozinov A, Hannula S-P, Lindroos VV (2005) Smart Mater Struct 14:223
4. Entel P, Buchelnikov VD, Khovailo VV, Zayak AT, Adeagbo WA, Gruner ME, Herper HC, Wassermann EF (2006) J Phys D: Appl Phys 39:865
5. Krenke T, Acet M, Wassermann EF, Moya X, Mañosa L, Planes A (2006) Phys Rev B 73:174413
6. Krenke T, Duman E, Acet M, Wassermann EF, Moya X, Mañosa L, Planes A, Suard E, Ouladdiaf B (2007) Phys Rev B 75:104414

7. Chernenko V, Segui C, Cesari E, Pons J, Kokorin V (1998) Phys Rev B 57:2659
8. Kresse G, Furthmüller J (1996) Phys Rev B 54:11169
9. Kresse G, Joubert D (1999) Phys Rev B 59:1758
10. Perdew JP, Burke K, Ernzerhoff M (1996) Phys Rev Lett 77:3865
11. Koepernik K, Eschrig H (1999) Phys Rev B 59:1743
12. Opahle I, Koepernik K, Eschrig H (1999) Phys Rev B 60:14035
13. http://www.fplo.de
14. Eschrig H, Richter M, Opahle I (2004) In: Schwerdtfeger P (ed) Relativistic electronic structure theory, Part II. Applications, Vol. 14 of theoretical and computational chemistry, Elsevier, pp 723–776
15. Perdew JP, Wang Y (1992) Phys Rev B 45:13244
16. Enkovaara J, Ayuela A, Nordström L, Nieminen RM (2002) Phys Rev B 65:134422
17. Ayuela A, Enkovaara J, Nieminen RM (2002) J Phys: Condens Matter 14:5325
18. Zayak A, Entel P, Hafner J (2003) J Phys IV 112:985
19. James RD, Hane KF (2000) Acta Mater 48:197
20. Bhattacharya K (2003) Microstructure of martensite—why it forms and how it gives rise to the shape-memory effect. Oxford University Press, Oxford
21. Pitteri M, Zanzotto G (2003) Continuum models for phase transitions and twinning in crystals. Chapman & Hall/CRC, Boca Raton
22. Ball JM, James RD (1987) Arch Rat Mech Anal 100:13
23. Bain EC (1926) Trans AIME 70:25
24. Pond RC, Celotto S (2003) Int Mater Rev 48:225
25. Kakeshita T, Fukuda T, Takeuchi T (2006) Mater Sci Eng A 438–440:12
26. Okamoto N, Fukuda T, Kakeshita T, Takeuchi T (2006) Mater Sci Eng A 438–440:948
27. Kakeshita T, Fukuda T (2006) Int J Appl Electrom 23:45
28. Kokalj A (2003) Comp Mater Sci 28:155; http://www.xcrysden.org